Formability and Defect Formation Mechanisms for a Binder-Stabilized Unidirectional Non-Crimp Fabric

Z. Mohammadi[1*] and J. Montesano[1]

[1] Composites Research Group, Department of Mechanical and Mechatronics Engineering, University of Waterloo, Waterloo, Canada.

* *Corresponding author (zohreh.mohammadi@uwaterloo.ca)*

Keywords: *Binder-stabilized unidirectional non-crimp fabric; Fabric preforming; Inter-layer interaction; Forming-induced defects*

1. Abstract

Unidirectional non-crimp fabrics (UD-NCFs) comprising stabilizing binder are more frequently considered for structural composites owing to their nearly crimp-free architecture and high lightweighting potential. However, UD-NCFs exhibit low stability during handling and are prone to forming-induced defects such as wrinkling. This study investigates the effect of binder state on the forming behavior of a carbon fiber UD-NCF using hemispherical and pyramidal punch forming tests. Three fabric conditions are examined: non-bindered, with binder inactivated, and with binder preactivated. Single-layer and double-layer specimens are tested under different contact configurations and fiber orientations, where the force-displacement response and local defects are assessed. The binder state was found to markedly affect both forming resistance and defect development. The non-bindered fabric exhibits lower forming forces and smoother deformation, indicating greater tow mobility, while the for the bindered fabric conditions forming resistance increases and localized wrinkling was promoted. These effects are more pronounced in double-layer and pyramidal forming, where binder stabilization restricts inter-ply sliding and promotes more collective deformation of the fabric stack. Overall, the results show that UD-NCF preforming is governed by multiple coupled mechanisms, including the binder state, which must be considered in future high-fidelity forming simulation models.

2. Introduction

Liquid composite molding processes are widely used for manufacturing high-performance composite structures, particularly when part geometries are complex [1,2]. In these processes, preforming of dry fabric layers into the desired 3D net shape prior to resin injection is typically performed [3,4]. The deformation states introduced during preforming directly affect the local fiber orientation, fabric architecture, compaction state, and permeability of the reinforcement, and therefore influences both manufacturability and final mechanical performance [5]. During preforming, initially flat textile reinforcements must conform to complex tooling, often involving double-curvature surfaces. This can generate large and non-uniform deformations, including in-plane shear and bending, inter-ply sliding, and local compaction [6]. If the reinforcement cannot accommodate the imposed deformation, forming-induced defects such as out-of-plane wrinkling, folding, fiber misalignment, and local distortion may occur [7].

Understanding the deformation mechanisms that govern fabric formability is therefore essential for optimizing forming processes and developing reliable forming simulation models [8]. Unidirectional non-crimp fabrics (UD-NCFs) are attractive for structural composites because their nearly crimp-free architecture provides improved in plane mechanical performance and greater lightweighting potential when compared to traditional woven reinforcements [9]. However, the absence of yarn interlacement and the directional stiffness of UD-NCFs limit their ability to accommodate complex deformation during preforming. As a result, UD-NCFs may exhibit characteristic forming-induced defects such as tow gapping and sliding, mesoscopic tow buckling, and macroscopic out-of-plane wrinkling, particularly when formed over double-curvature geometries [10]. Furthermore, UD-NCFs often comprise stabilizing binders to improve handleability during processing and enable preforming. However, binder activation can also modify deformation resistance by changing tow mobility, inter-tow interactions, and local stiffness [11]. As a result, binder state may influence both the global forming force response and the local development of forming induced defects.

Several experimental studies have investigated forming-induced defects in woven and multiaxial textile reinforcements. Hemispherical and punch-forming experiments on woven fabrics have demonstrated the influence of tool geometry, blank holder conditions, and process constraints on local shear and wrinkle formation [12,13]. Studies on biaxial NCFs have shown that wrinkle location is influenced by geometry, while wrinkle severity depends on fabric architecture and stitch configuration [14]. Although these studies provide valuable insight into textile forming, their conclusions are architecture-specific and cannot be directly transferred to UD-NCFs. Despite its practical importance, limited studies focused on the influence of binder state on the formability of UD-NCFs have been reported, particularly under different punch geometries and layer configurations. Accordingly, this study experimentally investigates the forming behavior of binder stabilized carbon fiber UD-NCFs under different binder states and forming conditions. The coupled effects of binder state, punch geometry, layer configuration, contact condition, and fiber orientation on force–displacement response and local defect formation are examined. The study aims to provide experimental insight needed for future high-fidelity macroscopic forming simulations.

3. Material and Experimental Methodology

3.1. UD-NCF Description

The reinforcement used in this study was a carbon fiber unidirectional non-crimp fabric, namely PX35-UD300 (Zoltek™). The fabric consisted of aligned tows each containing 50,000 PX35 carbon fibers, which were axially stitched with a polyester yarn in a tricot pattern. Transversely oriented glass fiber yarns provided the fabric with support during handling. One variant of the fabric did not contain a stabilizing binder, while the other variant consisted of a thermosetting powder binder. Additional architectural details of the fabric have been reported in previous studies [8, 15, 16]. The main fabric characteristics are summarized in Table 1. Note, the side of the fabric with the tricot stitch pattern visible (and the powder binder applied, as applicable) will be referred to as the ‘stitch side’, while the side of the fabric with the supporting glass fibers will be referred to as the ‘glass side’.

Table 1. ZoltekTM PX35-UD300 unidirectional non-crimp fabric characteristics

Parameter	**Value**
Total fabric areal density	$333\ g/m^2$
Carbon fiber tow weight fraction	92.8 %
Glass fiber yarn weight fraction	3.0 %
Glass fiber yarn linear density	34 dtex
Polyester stitch weight fraction	1.8 %
Polyester stitch linear density	76 dtex
Binder resin powder weight fraction	2.4 %
Nominal Carbon fiber diameter	7.2 µm

Three fabric conditions were investigated: non-bindered, with binder inactivated, and with binder preactivated. The with binder inactivated condition corresponded to the as received binder stabilized fabric, in which the thermosetting powder binder was present on the stitch side in solid powder form. The preactivated binder condition was prepared by heating the with binder fabric at 120 °C for 20 min between two aluminum plates, following the procedure reported in Ref. [17]. The non-binder condition corresponded to fabric manufactured without binder. Square fabric specimens measuring 400 × 400 mm were extracted from a roll and used for all forming tests.

3.2. Forming Test Setup

Forming experiments were conducted using a Shimadzu universal testing machine comprising a load cell with a ±100 lb capacity. The experimental setup consisted of interchangeable punch–die sets and a rigid support frame mounted to the base of the test machine (Figure 1). The die was secured to the support frame using clamps, while the punch was mounted to the load cell on the frame crosshead. A blank holder concentric with the cutout in the die was positioned on the specimen to enable controlled drawing of the fabric specimen, where the equivalent of 65 N of force was distributed on the blank holder. The support frame was designed to minimize vibration and maintain punch–die alignment.

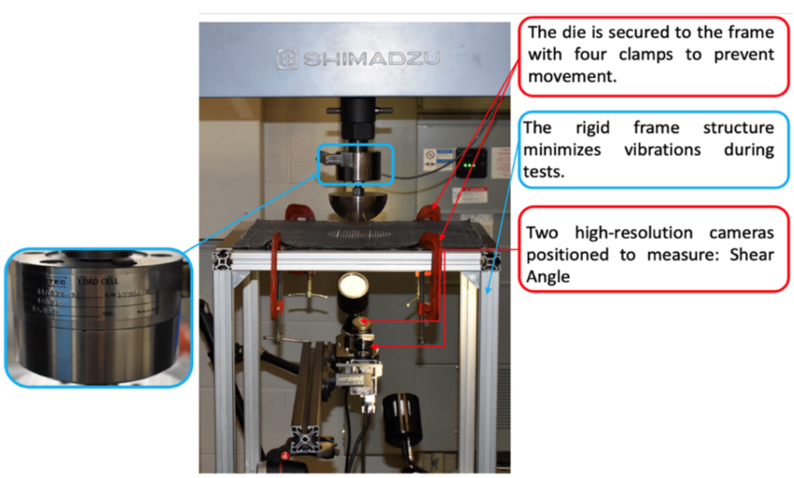

Figure 1. Experimental forming setup used for UD-NCF preforming tests, including the Shimadzu universal testing machine, punch–die assembly, rigid support frame, blank-holder/clamping system, secondary low-capacity load cell, and bottom-mounted camera system for deformation monitoring.

Two punch geometries were investigated: a hemispherical punch with a diameter of 100 mm and a square-base pyramidal punch. The corresponding die openings and blank holder geometries are shown in Figure 2. The steel punch, die, and blank holder surfaces had an average roughness of approximately 0.2 µm. Tests were performed in displacement control with a constant punch displacement rate of 1 mm/s. The measured response included punch force–displacement data and visual deformation observations.

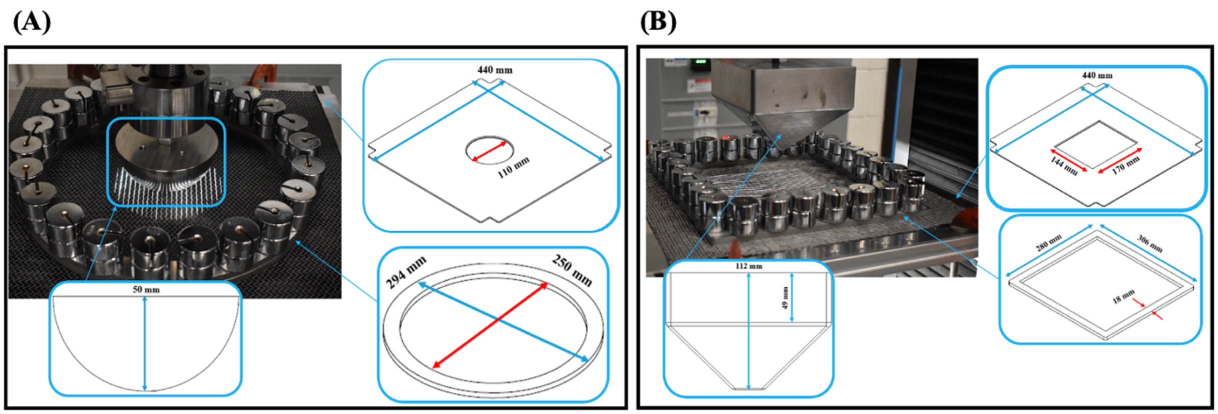

Figure 2. Forming tool geometries and specimen configurations: (A) hemispherical punch configuration; and (B) pyramidal punch configuration.

To evaluate the effects of stacking and contact condition, both single-layer and double-layer specimens were tested. Single-layer specimens were placed with either the glass or stitch side in contact with the punch, while double-layer specimens were arranged to create either glass–glass or stitch–stitch inter-ply contact. For tests performed with the pyramidal punch, the carbon fiber tows were oriented along the 0°, 45°, or 90° directions as shown in Figure 3. Forming tests for all conditions were repeated four times.

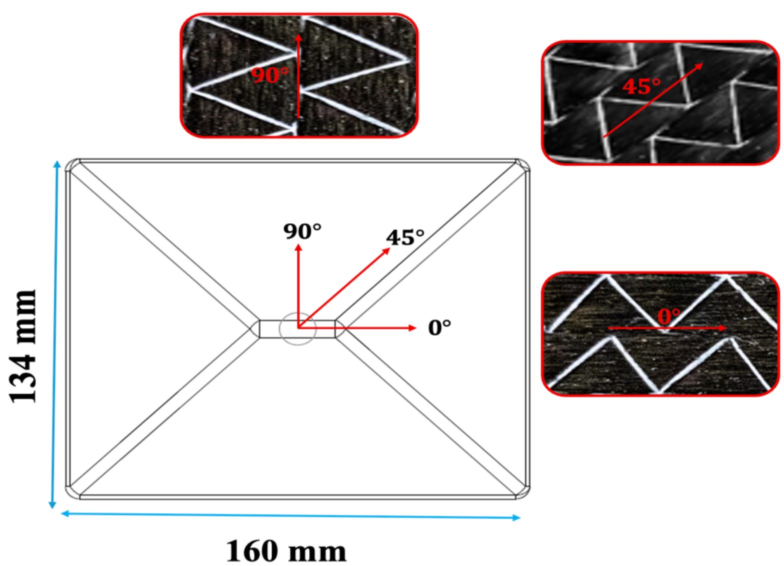

Figure 3. Pyramidal punch sharp-edge orientation relative to the UD-NCF carbon fibre direction in pyramidal forming tests: (A) 0°, (B) 90°, and (C) 45°.

4. Results

4.1. Effect of Binder State and Layer Configuration on Forming Response

The force–displacement response for single-layer UD-NCF specimens for each binder condition, with the stitch side placed in contact with the punch, revealed that the forming force increased nonlinearly with punch displacement (Figure 4). A progressive increase in deformation resistance was observed as the fabric initially conforms to the tooling as was then drawn into the die opening. A clear kink in the response for the pyramidal punch tests was observed at approximately 63 mm of punch displacement, which corresponds to the instant that the straight section of the punch reaches the die opening (Figure 2b). For the hemispherical punch, the bindered specimens exhibited substantially higher forming forces than the non-bindered specimens throughout most of the displacement range. At a punch displacement of 50 mm, the with binder inactivated condition reached the highest force, followed closely by the with binder preactivated condition, while the non-binder condition exhibited a considerably lower force response.

The effect of binder state was more pronounced for the pyramidal punch tests. The non-bindered specimen maintained a low forming force over most of the displacement range, whereas both binder stabilized specimens showed a continuous increase in force with displacement. The with binder inactivated specimens exhibited the highest force response, reaching approximately 100 N at a punch displacement of 80 mm, while for the with binder preactivated condition the force reached approximately 70 N. Although the with binder preactivated condition was expected to produce the highest resistance, this result indicates that binder activation did not increase the global forming force for all forming configurations. Overall, these results show that binder state strongly influences the forming response, particularly when the punch geometry imposes more localized deformation. Although not presented herein, the overall trends observed for the same conditions with the glass side of the fabric in contact with the punch were similar to those presented. However, the with binder preactivated specimens produced a higher force response than the with binder inactivated specimens.

The force–displacement response for double-layer UD-NCF specimens with stitch–stitch inter-ply interaction showed higher forming forces (Figure 5) when compared to the single layer specimens, which was expected given the greater resistance to deformation and friction between layers. For the hemispherical punch, the non-bindered condition exhibited the lowest force response, while the with binder inactivated and preactivated conditions exhibited higher forming resistance. The with binder preactivated specimen attained the highest force, approximately 120 N at a punch displacement of 50 mm.

For the pyramidal punch, the non-bindered specimen maintained a low force response over most of the displacement range, reaching approximately 20 N at a punch displacement of 80 mm. In contrast, the with binder inactivated and preactivated specimens showed a rapid increase in force at larger punch displacements, both reaching approximately 120 N. Although not presented herein, the trends observed for the same conditions with glass-glass inter-ply interaction were similar to those presented.

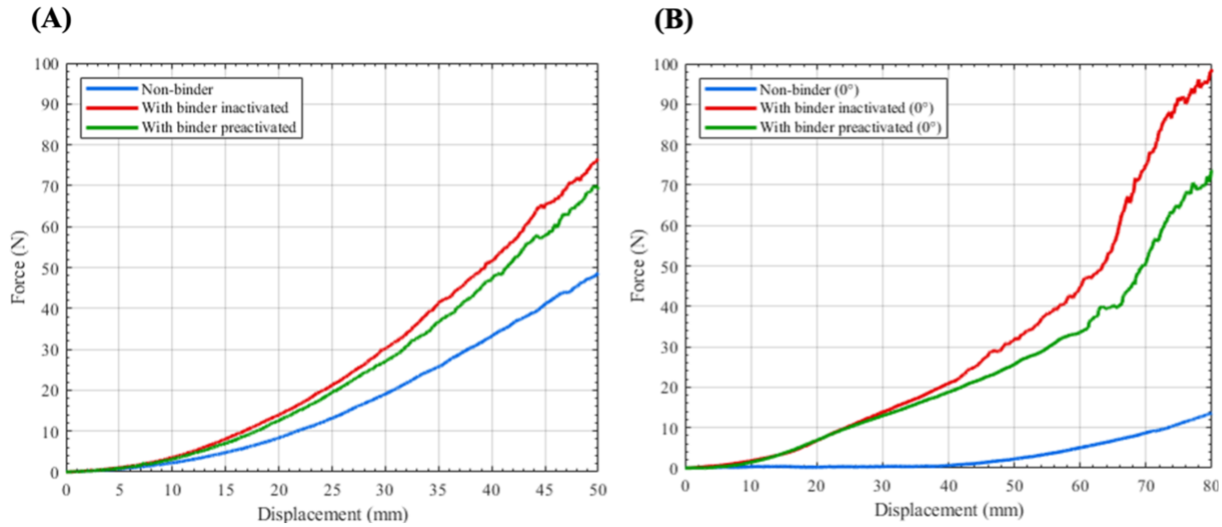

Figure 4. Average force–displacement response of single-layer UD-NCF specimens with the stitch side in contact with the punch: (a) hemispherical punch configuration, and (b) pyramidal punch configuration at 0° fibre orientation.

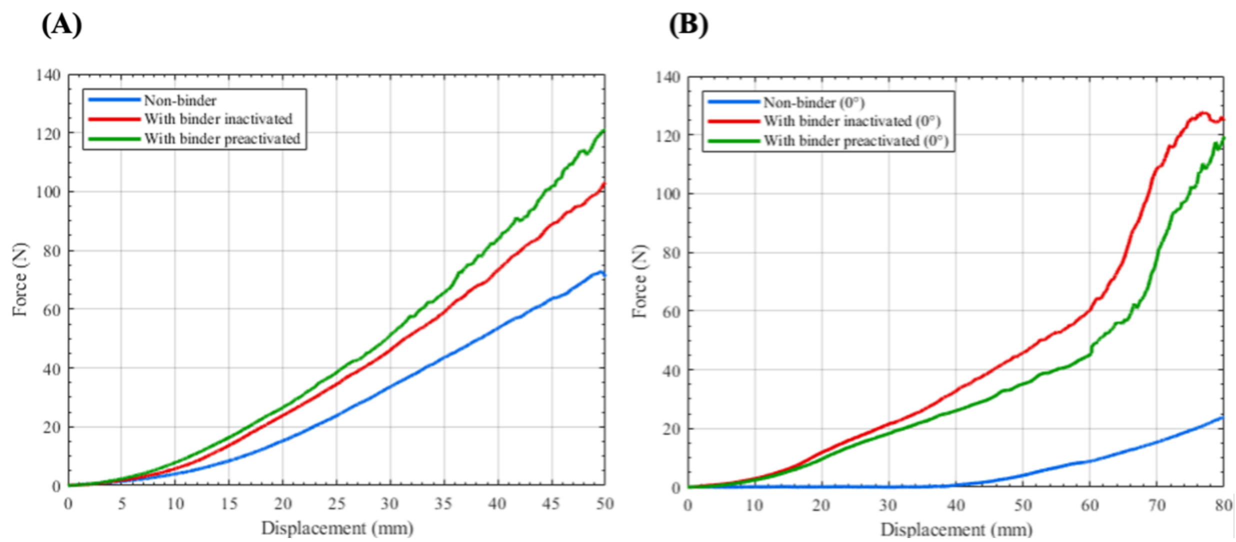

Figure 5. Average force–displacement response of double-layer UD-NCF specimens with stitch–stitch inter-ply interaction: (a) hemispherical punch configuration and (b) pyramidal punch configuration at 0° fibre orientation.

4.2. Effect of Binder State on Defect Formation

The single layer non-bindered specimens revealed comparatively smooth deformation during hemispherical forming, while the with binder inactivated and preactivated specimens showed more pronounced localized wrinkling (Figure 6). For the non-bindered specimens, the fabric was drawn through the die opening with less resistance owing to increased tow mobility, which prevented more pronounced wrinkling. In contrast, the with binder preactivated specimens exhibited sharper localized deformation, owing to restricted tow mobility and greater tow stiffness which promoted local transverse bending.

For the double-layer hemispherical specimens with stitch–stitch inter-ply interaction, the non-bindered specimens showed more distributed deformation and less resistance to inter-ply sliding, whereas the with binder inactivated and preactivated specimens showed greater deformation localization and more pronounced wrinkling (Figure 7). Compared with the single-layer specimens, the double-layer specimens showed stronger sensitivity to the binder state.

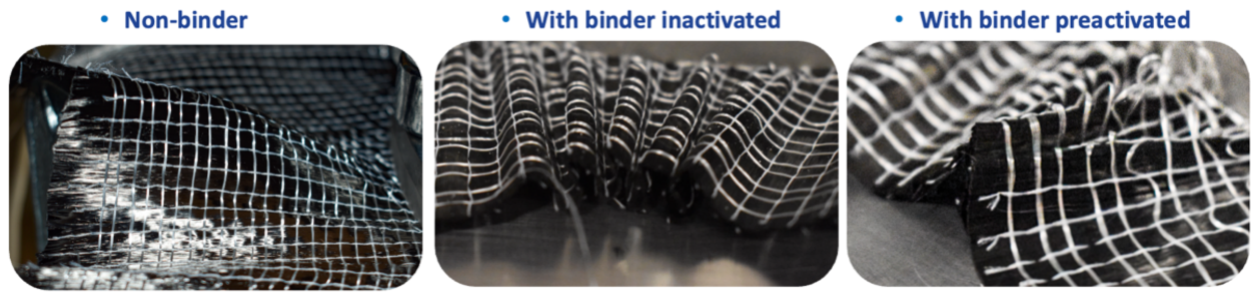

Figure 6. Representative fabric deformation at maximum punch displacement during single-layer hemispherical forming with the glass side in contact with the punch.

Figure 7. Representative fabric deformation at maximum punch displacement during double-layer hemispherical forming with stitch–stitch inter-ply interaction.

4.3. *Effect of Fiber Orientation on Forming Response*

The influence of fiber orientation was examined for tests performed using the pyramidal punch by comparing the response of single- and double-layer specimens with 0°, 45°, and 90° fiber orientations. Fiber orientation affected the forming force response; however, its influence depended on the state of the binder, layer configuration, and contact condition (Figure 8).

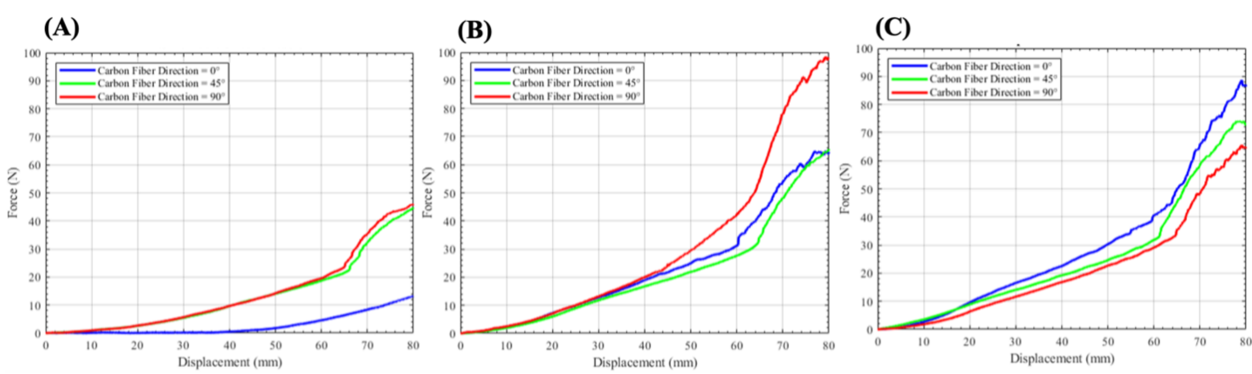

Figure 8. Average force–displacement response of single-layer UD-NCF specimens with the glass side in contact with the pyramid punch: (a) non-binder, (b) with binder inactivated, and (c) with binder preactivated.

For the single-layer specimens, the non-bindered fabric showed the strongest sensitivity to fiber orientation. For both stitch-side and glass-side punch contact conditions, the 0° orientation produced the lowest peak force (~14 N), while the 45° and 90° orientations produced notably higher forces (38–48 N). In contrast, the with binder preactivated specimens showed more consistent responses across all fiber orientations, particularly for stitch-side punch contact where all orientations reached peak forces of approximately 70–75 N. The with binder inactivated specimens generally produced higher forces; however, the dominant orientation was dependent on the contact side. Under stitch-side punch contact, specimens with 0° and 90° orientations achieved the highest peak forces (95–100 N), whereas under glass-side punch contact, specimens with 90° orientation produced the highest peak force (~98 N).

For the double-layer specimens, the influence of fiber orientation was more pronounced (Figure 9). The non-bindered specimens exhibited the lowest peak forces for the 0° orientation (22–25 N), while the 45° and 90° orientations achieved higher peak forces (58–70 N). The with binder preactivated specimens were least sensitive to fiber orientation with all orientations reaching peak forces in the range 115–130 N. The with binder inactivated specimens produced the highest forces and a strong dependence on orientation and contact condition, with final forces ranging from approximately 105 N to 180 N.

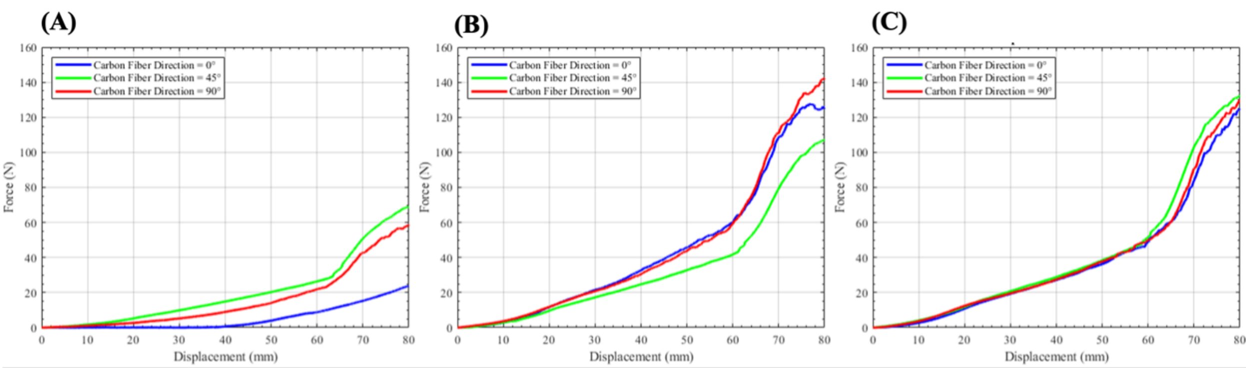

Figure 9. Average force–displacement response of double-layer UD-NCF specimens with stitch–stitch inter-ply interaction under pyramidal punch forming: (a) non-binder, (b) with binder inactivated, and (c) with binder preactivated.

These findings indicate that the pyramidal forming response is governed by the combined effects of fiber orientation, binder state, layer configuration, and contact condition, rather than fiber orientation alone.

5. Discussion and Conclusions

While it was expected that the forming response of the studied UD-NCF is dependent on the punch geometry, number of layers, and fiber orientation, the observed influence of binder state on the force-displacement response and local wrinkle formation was an important outcome of this study. The non-bindered fabric specimens exhibited markedly lower peak forces when compared to the bindered fabric specimens for all punch geometries, layer configurations, and contact conditions considered, owing to the increase in deformation resistance caused by the binder. Decreased tow mobility and increased tow stiffness for the binder stabilized fabrics also lead to increased local transverse bending and more pronounced out-of-plane wrinkling. It is interesting to note that the pyramidal punch forming experiments revealed a greater sensitivity to the binder state, revealing a coupled geometric and binder state effect. The fabric was allowed to macroscopically bend during the initial stage of the test, and more locally deform once the straight portion of the pyramidal punch reached the die opening. It is plausible that the bindered fabric specimens exhibited greater resistance to macroscopic bending deformation and local deformation during the first and second stages, showing a more marked increase in force. Another interesting result is that the with binder inactivated and preactivated specimens did not exhibit markedly distinct forming response, albeit the corresponding peak forces for each state were distinct. For the single layer forming experiments with stitch side in contact with the punch, the with binder preactivated specimens exhibited slightly lower peak forces, suggesting that the existence of inactivated powder binder on the stitch side may increase surface-level resistance at the punch contact to a greater extent than when the binder is preactivated.

Another important outcome of this study for the pyramidal punch tests was that the degree of influence of fiber orientation on the forming response was dependent on the binder state, number of layers, and contact condition. The peak forces measured for the non-bindered single-layer fabric specimens were greater for 45° and 90° fiber orientations, which is a result of distinct triggered deformation modes (e.g., tow rotation and transverse tension) when compared to the specimens with 0° fiber orientation. In contrast, the single-layer bindered fabric specimens exhibited more consistent peak forces for all fiber orientations, which may be attributed to greater resistance to fabric deformation caused by the binder and, thus, less influence of fiber orientation.

The results of this study provide the first foundational understanding of the influence of binder state on the formability of UD-NCFs, which will be built upon in future studies. Furthermore, the data generated in this study will be used to inform future macroscopic forming simulations to support process optimization and structural simulation of as-manufactured composite components.

6. References

[1] M. Deléglise, P. Le Grognec, C. Binetruy, et al., “Modeling of high-speed RTM injection with highly reactive resin with on-line mixing,” Composites Part A: Applied Science and Manufacturing, vol. 42, no. 10, pp. 1390–1397, 2011.

[2] B. Schäfer, R. Zheng, J. Colmars, A. Platzer, N. Naouar, P. Boisse, and L. Kärger, “Experimental analysis of the forming behavior of uni- and bidirectional non-crimp fabrics for different geometries,” Composites Part B: Engineering, vol. 287, p. 111765, 2024.

[3] A. Gasser, P. Boisse, and S. Hanklar, “Mechanical behavior of dry fabric reinforcements. 3D simulations versus biaxial tests,” Computational Materials Science, vol. 17, no. 1, pp. 7–20, 2000.

[4] S. Allaoui, J. Launay, D. Soulat, et al., “Experimental tool of woven reinforcement forming,” International Journal of Material Forming, vol. 1, suppl. 1, pp. 815–818, 2008.

[5] S. Allaoui, G. Hivet, D. Soulat, et al., “Experimental preforming of highly double curved shapes with a case corner using an interlock reinforcement,” International Journal of Material Forming, vol. 7, no. 2, pp. 155–165, 2014.

[6] T. Gereke, O. Döbrich, M. Hübner, et al., “Experimental and computational composite textile reinforcement forming: A review,” Composites Part A: Applied Science and Manufacturing, vol. 46, pp. 1–10, 2013.

[7] L. Kärger, S. Galkin, E. Kunze, M. Gude, and B. Schäfer, “Prediction of forming effects in UD-NCF by macroscopic forming simulation—Capabilities and limitations,” in Proc. 24th Int. Conf. Material Forming (ESAFORM 2021), 2021, doi: 10.25518/esaform21.355.

[8] M. Ghazimoradi and J. Montesano, “Macroscopic forming simulation for a unidirectional non-crimp fabric using an anisotropic hyperelastic material model,” Applied Composite Materials, vol. 30, no. 6, pp. 2001–2023, 2023.

[9] F. J. Schirmaier, K. A. Weidenmann, L. Kärger, et al., “Characterization of the draping behavior of unidirectional non-crimp fabrics (UD-NCF),” Composites Part A: Applied Science and Manufacturing, vol. 80, pp. 28–38, 2016.

[10] Y. Ali, A. Faisal, A. Saifullah, H. N. Dhakal, S. Alimuzzaman, and F. Sarker, “Fabrication and mechanical performance of non-crimp unidirectional jute-yarn preform-based composites,” Molecules, vol. 26, no. 21, p. 6664, 2021.

[11] R. M. Portela, B. Schäfer, L. Kärger, A. R. de Faria, and J. Montesano, “Effect of loading rate, viscosity, and binder activation on the bending response of an infiltrated UD-NCF,” Composites Part A: Applied Science and Manufacturing, vol. 200, Art. no. 109347, 2026, doi: 10.1016/j.compositesa.2025.109347.

[12] S. Chen, O. P. L. McGregor, L. T. Harper, A. Endruweit, and N. A. Warrior, “Defect formation during preforming of a bi-axial non-crimp fabric with a pillar stitch pattern,” Composites Part A: Applied Science and Manufacturing, vol. 91, pp. 156–167, 2016, doi: 10.1016/j.compositesa.2016.09.016.

[13] G. D. Lawrence, Automated forming of multi-ply non-crimp fabric structures, Ph.D. dissertation, University of Nottingham, Nottingham, U.K., 2024.

[14] C. Jiménez Martín, “A study of the pyramid of testing for forming of non-crimp fabrics for aerostructures,” Ph.D. dissertation, University of Bristol, Bristol, U.K., 2023.

[15] J. Montesano, M. Ghazimoradi, and V. Carvelli, “Characterizing and modelling the coupled in-plane shear-biaxial tension deformation response of unidirectional non-crimp fabrics,” International Journal of Material Forming, vol. 16, no. 4, 2023.

[16] M. Ghazimoradi, E. A. Trejo, V. Carvelli, et al., “Deformation characteristics and formability of a tricot-stitched carbon fiber unidirectional non-crimp fabric,” Composites Part A: Applied Science and Manufacturing, vol. 145, 2021.

[17] R. Miranda Portela, B. Schäfer, L. Kärger, et al., “Influence of viscosity, binder activation, and loading rate on the membrane response of an infiltrated UD-NCF,” Materials Research Proceedings, pp. 494–502, 2024.